X-ray Absorption Spectroscopy of the Iron Site in *Escherichia coli* Fe(III) Superoxide Dismutase†

David L. Tierney,‡ James A. Fee,§ Martha L. Ludwig,|| and James E. Penner-Hahn*,‡

Department of Chemistry, University of Michigan, Ann Arbor, Michigan 48109-1055, Department of Biology, University of California, San Diego, La Jolla, California 92037, and Department of Biological Chemistry and Biophysics Research Division, University of Michigan, Ann Arbor, Michigan 48109-1055

Received July 7, 1994; Revised Manuscript Received November 2, 1994®

ABSTRACT: The local structure of the iron site in ferric superoxide dismutase from *Escherichia coli* has been characterized by X-ray absorption spectroscopy. In the resting state of the enzyme at pH 7.0, the iron is five-coordinate with an average metal−ligand bond length of 1.98 Å. Binding of azide causes a reduction in the intensity of the bound state 1s→3d transition and an increase of 0.08 Å in average bond length. Both are indicative of an increase in the iron coordination number. Raising the pH from 7.0 to 10.5 causes a similar 0.08 Å increase in the average bond length, again suggesting an increase in the iron coordination number. At intermediate pH (9.4), the average bond length is 2.03 Å, consistent with an approximately 50:50 mixture of the limiting high and low pH forms. Similarly, the absorption edge structure varies continuously from pH 7 to 10.5. These spectra can be fit to a titration curve with a pK_a of approximately 9.8. These data suggest that the pH-dependent transition, previously identified by UV−vis, EPR, and activity measurements, may be the conversion of the iron from five- to six-coordinate, presumably through coordination by hydroxide. The 1s→3d transition for ferric superoxide dismutase at high pH is broader but not significantly less intense than that at pH 7. This suggests that the high pH form may be significantly distorted from octahedral symmetry. At pH 7, the ferric and ferric + azide samples undergo slow X-ray induced photoreduction. The amount of Fe(II) produced was estimated at less than 20% at the end of data collection. The samples measured at elevated pH showed no signs of photoreduction.

Superoxide dismutases (SODs),[1] which catalyze the disproportionation of superoxide to hydrogen peroxide and dioxygen, have been implicated in the protection of cells from spurious oxidative damage. Three forms of the enzyme are known, differing in the type of metal required for activity. However, there are only two distinct types of protein structures. The Cu/Zn protein, the first structure to be determined, contains one copper and one zinc ion per 17 kDa monomer and is found primarily in the cytosol of eukaryotic cells (Roberts et al., 1991). Proteins that utilize a single Fe or Mn at their active sites constitute the second structural class and are widely distributed in bacteria (Fe- or MnSODs) (McCord & Fridovich, 1969; Sato & Nakasawa, 1978; Autor, 1982) and in the mitochondria (MnSOD) of eukaryotic cells (Borgstahl et al., 1992). In each case, catalysis appears to follow the scheme

$$E_{ox} + O_2^- \rightarrow E_{red} + O_2 \quad (1)$$

$$E_{red} + O_2^- + 2H^+ \rightarrow E_{ox} + H_2O_2 \quad (2)$$

with the individual rates being greater than 10^8 M^{-1} s^{-1}.

A series of crystallographic analyses of Mn^- and Fe SODs show the enzymes to be structurally similar (Ringe et al., 1983; Stallings et al., 1983, 1985, 1991, 1992; Carlioz et al., 1988; Stoddard et al., 1990a,b; Ludwig et al., 1991) to one another but structurally unrelated to the Cu/Zn proteins. In both Mn- and FeSODs the metal is coordinated to three histidine nitrogens and one aspartate oxygen, with several conserved aromatic residues enveloping the active site. In particular, recombinant MnSOD from human mitochondria (Borgstahl et al., 1992) has a metal site that is nearly indistinguishable from that of the *Escherichia coli* Fe and *Thermus thermophilus* Mn enzymes. The crystal structures for the *E. coli* (Stallings et al., 1983) and *Pseudomonas ovalis* (Ringe et al., 1983) FeSODs show similar primary structure and the same overall protein fold. The structure for the *E. coli* Fe enzymes shows a trigonal bipyramidal iron with two histidines and one aspartate as equatorial ligands and axially coordinated solvent and histidine. In contrast, the geometry of metal ligation described for *P. ovalis* FeSOD (Ringe et

† This work was supported in part by the National Institutes of Health (GM-38047 to J.E.P.H.; GM-16429 to M.L.L.; and GM-35189 to J.A.F.). The XAS spectra described in this paper were measured at SSRL and NSLS. SSRL and NSLS are operated by the Department of Energy, Office of Basic Energy Sciences, Division of Chemical Sciences, with additional support from the NIH, Biomedical Resource Technology Program, Division of Research Resources and the Department of Energy, Office of Health and Environmental Research. Data at NSLS were measured at beamlines X9 and X19A. X9 is supported by the NIH Division of Research Resources. Beamline X19A was supported in part by the Office of the Vice President for Research, University of Michigan.

* Author to whom correspondence should be addressed.

‡ Department of Chemistry, University of Michigan, Ann Arbor.

§ University of California, San Diego.

|| Department of Biological Chemistry and Biophysics Research Division, University of Michigan, Ann Arbor.

® Abstract published in *Advance ACS Abstracts,* January 15, 1995.

[1] Abbreviations: SOD, superoxide dismutase; XAS, X-ray absorption spectroscopy; EXAFS, extended X-ray absorption fine structure, XANES, X-ray absorption near-edge structure; FT, Fourier transform; EPR, electron paramagnetic resonance.

0006-2960/95/0434-1661$09.00/0

al., 1983) shows the iron to be coordinated by the same four protein ligands but distorted toward a tetrahedral arrangement with little or no evidence for coordination of solvent. In addition, there are dramatic variations in metal-ligand distances, with the *E. coli* and the *P. ovalis* structures having average iron−ligand distances of 2.0 and 2.4 Å, respectively.

Several anions act as inhibitors of FeSOD (Fee et al., 1981; Bull & Fee, 1985), and spectroscopic studies indicate that some of these inhibitors perturb the active site environment. While large anionic inhibitors such as perchlorate do not alter the spectral properties of the enzyme, smaller anions such as azide and fluoride produce spectral changes suggestive of coordination to the iron (Slykhouse & Fee, 1976; Villafranca, 1976; Fee et al., 1981; Dooley et al., 1987). Presumably, the larger anions inhibit the enzyme by blocking access to the substrate channel, while the smaller anions form inner sphere complexes with the iron (Stallings et al., 1991, 1992). Azide, a good mimic for molecular oxygen, is believed to bind in the same way as superoxide. The crystal structures of the azide derivatives of both the *E. coli* (Stallings et al., 1991) and *P. ovalis* (Stoddard et al., 1990b) FeSOD have been determined. Neither structure shows displacement of protein ligands upon binding of azide, and both suggest expansion of the iron coordination sphere.

Ferric SOD shows two pH-dependent spectral perturbations in its EPR and visible absorption spectra, with apparent pK_a values of 5.1 and 9.0 (Fee et al., 1981). These spectral changes are associated with changes in the catalytic activity of the enzyme. The Michaelis constant, K_m, is strongly dependent on pH above pH 8. Similarly, the K_d for azide binding increases above pH 7.5, with an apparent pK_a of 8.6. The high pH transition is linked to the loss of one proton and was originally attributed to the deprotonation of a bound water (Bull & Fee, 1985). More recently, it has been suggested (Stallings et al., 1991) that the high pH transition could be due to binding of exogenous hydroxide ion to form a six-coordinate iron site.

X-ray absorption spectroscopy (XAS) provides a sensitive probe of the local structural environment of metal ions in metalloproteins. Because it can provide higher resolution structural information than is available from protein crystallography, XAS is an important complement to crystallographic studies. Protein crystallography can typically give metal−ligand distances with an accuracy of ca. ±0.10 Å. This accuracy is of the same magnitude as the changes in bond length that are seen for Fe(III) complexes on going from four- to five-coordinate or five- to six-coordinate[2] (Shannon, 1976; Thorp, 1992). In contrast, extended X-ray, absorption fine structure (EXAFS, ca. 50−1000 eV above the edge) provides direct determination of the average metal−ligand bond distance with an accuracy of ±0.02 Å and a precision of ±0.005 Å. This accuracy is sufficiently good that the average EXAFS bond length can be used to distinguish between four-, five-, and six-coordinate sites.[3]

[2] The ionic radii for high spin Fe(III) complexes are 0.49 Å (four-coordinate), 0.58 Å (five-coordinate), and 0.65 Å (six-coordinate) (Shannon, 1976).

[3] A survey of the Cambridge Structural Database for high spin Fe(III) complexes with mixed N/O ligation gave an average bond length of 1.99 ± 0.02 Å for five-coordinate and 2.05 ± 0.02 Å for six-coordinate. Few four-coordinate Fe(III) complexes are known. However, the expected bond length for an FeN_3O structure, such as that predicted for the *P. ovalis* FeSOD, is <1.9 Å.

In addition, the X-ray absorption near edge structure (XANES) region (±25 eV about the absorption edge) provides information about geometry and oxidation state. In order to characterize in more detail the local structure of the metal site in FeSODs, we have undertaken an XAS study of *E. coli* FeSOD. We report here the XAS spectra for the ferric enzyme at neutral pH, for its corresponding azide complex, and for its high pH derivatives. The implications of these results with respect to the FeSOD catalytic cycle are discussed.

EXPERIMENTAL PROCEDURES

Superoxide dismutase was purified in Los Alamos according to published procedures (Slykhouse & Fee, 1976) and shipped to Ann Arbor on dry ice. The enzyme was allowed to stand exposed to air at 4 °C for ~24 h to give homogeneous ferric enzyme. All samples were prepared with 25% (v/v) glycerol as a glassing agent, loaded in Lucite curvettes with 6 μm polypropylene windows, and frozen rapidly in liquid nitrogen. EXAFS samples of the ferric enzyme were 3−5 mM in protein with approximately 80% occupation of the iron sites (2−4 mM Fe, based on A_{350}/A_{280}) in 10 mM Tris·Cl, pH 7.0. The protein was treated with EDTA to complex nonspecifically bound iron, which was subsequently removed by ultrafiltration with a Centricon 10 microconcentrator. The azide complex was prepared by adding 70 μL of 100 mM sodium azide in 10 mM Tris·Cl at pH 7.0 to 70 μL of protein and concentrating back to 70 μL. The K_d of azide is 1−2 mM; thus >92% of the iron sites have azide bound under these conditions. Binding of a second azide to form a red complex was not observed. Ferric SOD at pH 9.4 was prepared by slowly adding to 70 μL of enzyme in Tris·Cl, pH 7, an equal volume of 10 mM Tris at pH 13 with rapid mixing and subsequent ultrafiltration. The pH 8.5 derivative was prepared by dialyzing FeSOD, pH 7.0, against 10 mM Tris·Cl at pH 8.5 for 12 h. The higher pH samples (pH 9.9 and 10.5) were prepared by first dialyzing to pH 8.5 and finally dialyzing against 10 mM Tris at the desired pH. The final pH of all samples was verified with a microelectrode (Microelectrodes, Inc., Londonderry, NH). Fully reduced ferrous enzyme was obtained by slow addition of an anaerobic solution of 10 mM sodium dithionite with rapid mixing. The integrity of all samples was confirmed by their UV−visible spectra.

X-ray absorption spectra were measured at the Stanford Synchrotron Radiation Laboratory beamline VII-3, using a Si(220) double crystal monochromator, and at the National Synchrotron Light Source, using beamlines X19A with a Si(111) double crystal monochromator and X9A with a Si(220) double crystal monochromator. At beamlines VII-3 and X19A, the monochromator was detuned 50% for harmonic rejection. Beamline X9A employed an upstream focusing mirror for harmonic rejection. All data were measured as fluorescence excitation spectra with a 13-element solid-state Ge detector array. The detectors were run at a total incident count rate of <40 kHz per channel. The windowed count rates (Fe Kα fluorescence) were 1−3 kHz per channel. Samples were held at 10 K in an Oxford liquid He cryostat (beamlines VII-3 and X19A) or at 18 K in a Displex cryostat (beamline X9A) during XAS measurements.

EXAFS spectra were measured with 10 eV steps below the edge (6900−7100 eV), ~0.3 eV steps in the edge region

(ca. 7100−7150 eV) and 0.05 Å^{-1} steps in the k range 2−13 Å^{-1}. Integration times varied from 1s in the pre-edge region to 20 s at k = 13 Å^{-1} for a total integration time of approximately 35−40 min per scan. For the intermediate pH samples, where only the XANES region was analyzed, the scan protocol was modified to use steps of 0.1 Å^{-1} above the edge (k = 2−10 Å^{-1}) with integration times of 2 s per point, for a total integration time per scan of approximately 30 min. Total exposure time was typically 6 h for EXAFS samples and approximately 1 h for XANES samples.

Individual scans from each detector channel were examined to confirm the absence of artifacts and averaged to give the final spectra. The EXAFS spectra represent the average of 8−12 scans, each scan being the average of 8−11 channels. For samples where only the XANES spectra were measured, two scans were averaged. Total Fe Kα fluorescence counts ranged from ~1 to 6 × 10^6 at k = 13 Å^{-1} for the EXAFS scans and were ~80 000 in the XANES region for XANES scans. X-ray energies were calibrated by reference to the absorption spectra of an iron foil measured at the same time as the protein data. The first inflection point of the Fe foil was assigned as 7111.2 eV.

XANES spectra were analyzed by first normalizing the spectra to match the tabulated X-ray absorption cross-section (McMaster et al., 1969) below and well above the edge using a single cubic polynomial and a scale factor (Waldo, 1991). The 1s→3d pre-edge transition was isolated by fitting a second-order polynomial plus an arctangent to the regions immediately below (7100−7109 eV) and above (7117−7125 eV) the transition. This background function was then subtracted from the data to leave the 1s→3d transition. Areas were calculated by trapezoidal integration (7105−7122 eV) and normalized by dividing by the edge jump.

EXAFS background subtraction was accomplished by fitting a first-order polynomial to the pre-edge region and a two region cubic spline above the edge. Data were converted from energy to k space using $k = \sqrt{2m_e(E-E_0)/\hbar^2}$ with E_0 set at 7130 eV. The resultant EXAFS data were Fourier transformed over the range k = 1.5−11.8 Å^{-1}, except the pH 10.5 data (Δk = 1.5−11.3 Å^{-1}). The first shell was backtransformed [R = 0.80−1.95 Å (pH 7), 0.80−2.00 Å (pH 7 + azide), 0.80−2.00 Å (pH 9.4), and 0.75−2.00 Å (pH 10.5)] over the same k range. The resulting EXAFS data (ca. 8 degrees of freedom) were fit to eq 3 by using a

$$\chi(k) = \sum \frac{N_s A_s(k) S_c}{kR_{as}^2} \exp(-2K^2 \sigma_{as}^2) \exp(-2R_{as}/\lambda) \sin[2kR_{as} + \phi_{as}(k)] \quad (3)$$

nonlinear least-squares algorithm.

In eq 3, N_s is the number of scattering atoms in a shell, $A_s(k)$ is the back-scattering amplitude of the absorber−scatterer pair, σ^2 is the mean square deviation of the absorber−scatterer bond length R_{as}, $\phi_{as}(k)$ is the phase shift, λ is the photoelectron mean free-path, and the sum is taken over all shells of scatterers contributing to the EXAFS. The parameter S_c is the scale factor, which is, in principle, specific to the absorber−scatterer pair. The program FEFF v. 3.25 (Rehr & Zabinsky, 1991) was used to calculate *ab initio* amplitude and phase functions, $A_s(k) \exp(-2R_{as}/\lambda)$ and $\phi_{as}(k)$. Calculations were done for an iron−nitrogen interaction at 2.00 Å, an iron−oxygen interaction at 1.90 Å, and an iron−sulfur interaction at 2.30 Å. The scale factor, S_c, and the shift in E_0 relative to 7130 eV were calibrated by fitting compounds of known structure. The models used for calibration were Fe(III)(dimethyldithiocarbamate)$_3$ for Fe−S and Fe(III)(TPP)(SO_3CF_3) and Fe(III)(salen)(acetate) for Fe−N/O. The optimum values obtained for all compounds were S_c = 0.9 and ΔE_0 = 10 for the first shell. Subsequent fits to the protein data, for all reasonable integer coordination numbers, were generated by allowing R and σ to vary while holding S_c and ΔE_0 fixed.

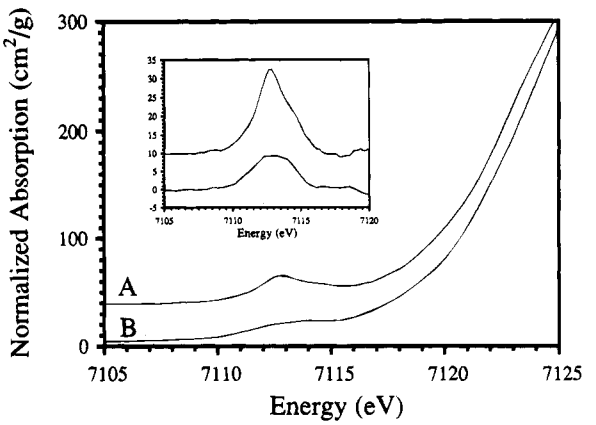

FIGURE 1: Normalized XANES spectra for ferric SOD (A) and ferric SOD + azide (B). Spectra have been offset for clarity. (Inset) Isolated 1s→3d transitions. The spectra in the inset appear in the same order as in the figure.

Table 1: XAS Results for Fe(III) SOD Derivatives at pH 7[a]

		CN[b]	R_{ab} (Å)	σ^2 (Å^2 × 10^{-3})[c]	1s→3d area[d]
ferric pH 7					
July 1992	SSRL VII-3	5 N/O	1.99	8.6	14.4
October 1992	NSLS X19A	5 N/O	1.99	10.7	16.7
January 1993	SSRL VII-3	5 N/O	2.00	11.1	15.4
ferric + azide					
October 1992	NSLS X19A	6 N/O	2.07	7.4	8.5
January 1993	SSRL VII-3	6 N/O	2.08	10.0	7.9

[a] The fits shown are for filtered first shell data. Fits to the unfiltered data gave similar results. The bond lengths have not been corrected for photoreduction. The data represent individual data sets for ferric SOD, with and without azide, collected from July 1992 to January 1993. [b] Integer coordination number giving the best fit. [c] Mean-square deviation in absorber−scatterer bond length. [d] Normalized 1s→3d peak areas in units 10^{-2} eV. The estimated uncertainty in areas is ±3 (see text).

RESULTS

Figure 1 shows the normalized absorption edges for ferric SOD, pH 7, with and without azide. The integrated 1s→3d areas for all samples are given in Table 1. Six separate measurements of the XANES (data not shown) for the ferric enzyme at pH 7 gave areas ranging from 12 to 18 × 10^{-2} eV. Most of this variability appears to result from uncertainties in the background function that is subtracted from the data. Despite the uncertainty in the integrations of the 1s→3d transition, a clear decrease in 1s→3d intensity on azide binding is apparent in both Figure 1 and Table 1.

The edges for the samples measured at pH 7 (ferric ± azide) are all shifted to slightly lower energy relative to the high pH samples. Comparison of the time dependence of the XANES spectra (Figure 2) revealed that this shift was due to slow photoreduction of the ferric enzyme at neutral pH. In order to quantitate the extent of photoreduction,

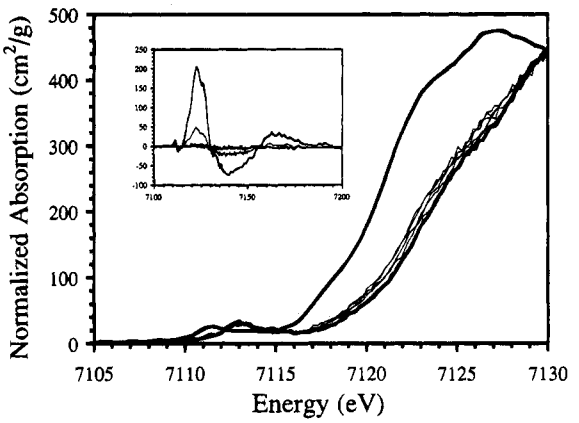

FIGURE 2: Time dependence of the XANES spectra for ferric SOD, pH 7. (Bold, right) Spectrum for first ferric scan. (Bold, left) Spectrum for ferrous enzyme. (Light lines) Scans 3, 5, 7, 10, and 12 in a series for ferric SOD showing slow production of Fe(II). (Inset) Difference spectra. (Bold) Ferrous minus first ferric scan. (Light) Last ferric scan minus first ferric scan showing production of ca. 20% Fe(II) during the experiment. (Dotted) Second ferric scan minus first ferric scan showing the amount of photoreduction per scan.

normalized difference spectra were calculated between the first scan for a sample and successive scans. These difference spectra have a characteristic bipolar shape (inset to Figure 2). To estimate the extent of photoreduction, the first ferric scan (during which negligible photoreduction occurs) was subtracted from the spectrum of the fully reduced protein. This difference signal was assigned as 100% ferrous. Individual ferric scans were then subtracted from the ferric scan, and the resulting difference signals were compared with the 100% ferrous signal. The rate of photoreduction was ~3% per hour, with less than 20% of the ferric iron being reduced during the course of data collection. Thus, the average of all of the scans represents protein that is ca. 90% in the ferric form. In contrast to the pH 7 samples, no detectable photoreduction occurred for the pH 9.4 and 10.5 samples. No detectable photoreduction was observed for the XANES samples, as expected, given the short (~1 h) measurement times for these samples.

A decrease in the height of the pre-edge transition, similar to that for the azide complex, is observed when the pH is raised. Figure 3a shows the normalized XANES spectra for ferric SOD as a function of pH. Although the 1s→3d transition clearly shows systematic variations with pH (inset to Figure 3A), the integrated area does not appear to change significantly (see Table 2). More importantly, the apparent 1s → 3d area does not change monotonically as the pH is increased. We attribute this behavior to difficulty in accurately integrating the 1s→3d area at high pH. In particular, the apparent area of the very broad transition at high pH is very sensitive to the background function used to model the rising edge.

As an alternative probe of pH-dependent structural changes, we calculated the second derivative of the XANES region. These spectra (Figure 3B) show a clear systematic variation as a function of pH. The minima in the second derivative spectra at ca. 7125−7130 eV are a measure of the curvature in the principal absorption maxima. The trend toward lower amplitude of this feature with increasing pH indicates a broadening of the absorption edge. The amplitude of the second derivative at 7129 eV as a function of pH is shown

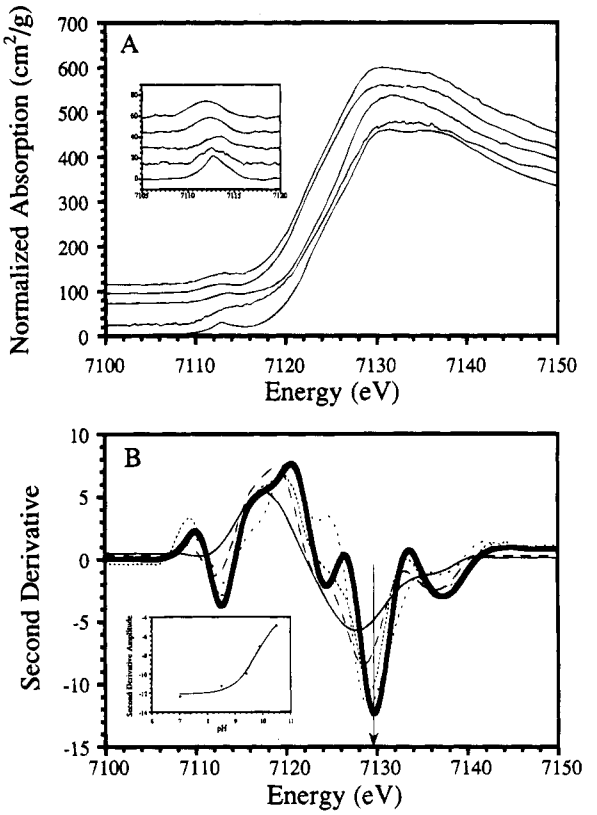

FIGURE 3: (A) Normalized XANES spectra for ferric SOD as a function of pH. The spectra have been offset for clarity and appear in the order, from bottom to top, pH 7.0, 8.5, 9.4, 9.9, and 10.5. (Inset to A) Isolated 1s→3d transitions as a function of pH. The spectra appear in the same order as in the figure. (B) Corresponding second derivatives of the XANES spectra shown in panel A. The arrow indicates the point used for the titration curve calculations. (Inset to B) XANES detected titration curve for ferric SOD. Smooth line is the best fit to eq 4 using $pK_a = 9.8$.

Table 2: XAS Results for Fe(III) SOD Derivatives[a]

sample	CN[b]	R_{ab} (Å)	σ^2 (Å^2 × 10^{-3})[c]	1s→3d area[d]	F[e]
pH7.0 (1)	5 N/O	1.98	12.1	15.8	0.30
(2)	2 O	1.90	7.1		0.20
	3 N	2.06	10.5		
pH 8.5				12.6	
pH 9.4	6 N/O	2.03	9.0	10.4	0.40
pH 9.9				14.0	
pH 10.5	6 N/O	2.05	8.9	14.6	0.25
pH 7.0 + azide	6 N/O	2.06	8.8	8.2	0.41

[a] The fits shown are for filtered first shell data. Fits to the unfiltered data gave similar results. The reported bond lengths are corrected for photoreduction (see text) giving slightly shorter bond lengths than seen in Table 1. The experimental precision in R_{ab} is 0.005Å. However, the estimated accuracy of the bond length is ±0.02 Å. For the pH 7 data, both one shell and two shell fit results are shown (see text). The data at pH 7 represent the overall averages for the data sets presented in Table 1. [b] Integer coordination number giving the best fit. [c] Mean-square deviation in absorber−scatterer bond length. [d] Normalized 1s→3d peak areas in units 10^{-2} eV. The estimated uncertainty in areas is ±3 (see text). [e] Goodness of fit (F) defined as $k^3\chi_{obs} - k^3\chi_{calc}$.

in the inset to Figure 3B. This trend can be modeled by assuming that the intermediate pH spectra (and hence the second derivative of these spectra) represent a superposition of the limiting low- and high-pH spectra. These data were fit to eq 4, where y is the second derivative amplitude, and c_1 and c_2 are empirical constants. The second derivative amplitude for the low pH form is represented by c_1, and the second derivative amplitude for the high pH form is given

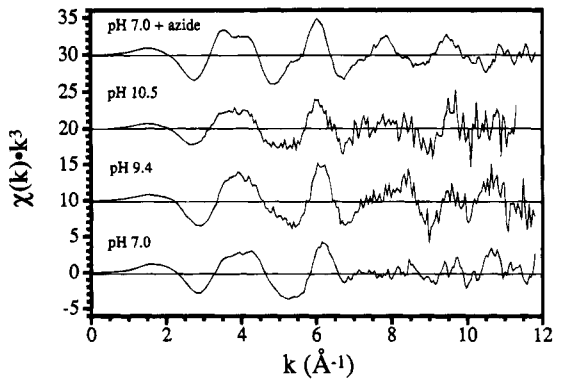

FIGURE 4: EXAFS data for FeSOD. From the bottom: ferric, pH 7; ferric, pH 9.4; ferric, pH 10.5; ferric + azide. Data were scaled by k^3 to enhance oscillations at high k. All spectra are plotted on the same scale with the upper spectra offset vertically by 10, 20, and 30 for clarity.

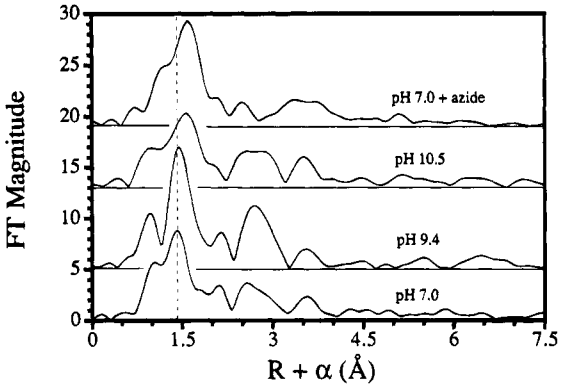

FIGURE 5: Fourier transforms of FeSOD EXAFS data shown in Figure 4. The spectra appear in the same order as in Figure 4 and are on the same scale, offset vertically.

by c_2. The best fit gave an apparent pK_a of 9.8 ± 0.2. The uncertainty in the pK_a was estimated by holding the pK_a fixed

$$y = \frac{c_1 10^{(\mathrm{pH}-\mathrm{p}K_a)} + c_2}{1 + 10^{(\mathrm{pH}-\mathrm{p}K_a)}} \quad (4)$$

while allowing the constants to vary. When pK_a is fixed at a value less than 9.6 or greater than 10, the quality of the fit decreases substantially.

EXAFS data for ferric SOD at pH 7 and for its azide complex were measured in three and two data sets, respectively, using two independently prepared samples of each derivative. Curve fitting results for individual data sets are summarized in Table 1. From these data, it is clear that the precision of the first shell bond length determination is excellent. Although multiple measurements were not made for the high pH samples, EXAFS data for these samples were of the same quality as each data set measured at pH 7. We therefore anticipate a comparable precision (±0.005 Å) at high pH.

Since the individual data sets at pH 7.0 gave identical structural results, they were averaged to obtain a better signal-to-noise ratio. The background subtracted EXAFS data and the corresponding Fourier transforms (FTs), shown in Figures 4 and 5, respectively, represent the overall averages for each sample. The data for the ferric protein and for its azide complex are the result of averaging a total of 40 and 28 scans, respectively. The data presented for the enzyme at pH 9.4 is the result of averaging 8 scans, and that for pH 10.5 represents the average of 12 scans. The low amplitude of the EXAFS data in Figure 4 is indicative of an iron site with primarily low-Z ligands. From both Figure 4 and Figure 5, it is evident that there is a structural change on binding azide. This is most apparent in the $k = 3-6$ Å^{-1} region of Figure 4. In Figure 5 there is a noticeable shift of the main peak to higher R and higher amplitude on azide binding. In order to estimate the uncertainty in the FT magnitude, the individual FTs from each data set for the ferric pH 7 and for the ferric + azide samples were averaged. The standard deviation in FT magnitude was 0.37 for the azide complex and 0.44 for the ferric pH 7. Within these error limits, the amplitude differences with and without azide are significant. The magnitude of the main peak in the FT for the ferric enzyme is 8.8, while that for the azide complex is 10.3. Such an increase is consistent with either an increase in coordination number or a decrease in disorder for the azide complex relative to the ferric pH 7 sample.

The FT for the ferric enzyme at pH 7 shows the outer shell scattering typical of imidazole coordination, with peaks at $R + \alpha \approx 2.8$ and 3.6 Å. Although clearly above the noise level of the data, the outer shells were not included in the present curve fitting analysis, as they are not critical to the information being sought. The FT of the azide bound form does not exhibit such clearly defined features and appears to have a new peak at $R + \alpha \approx 3.3$ Å. These differences, which are highly reproducible between data sets, may be the result of EXAFS contributions from the outer nitrogens of the azide. The FTs for the high pH samples also show outer shell scattering. There is however, greater variability in these peaks, most likely due to the lower signal-to-noise ratio of these spectra (see Figure 4).

Fits to first shell filtered EXAFS are shown in Figure 6. For all three data sets, the ferric pH 7 sample could be fit with a single shell of 5 N at 1.99 Å or with two shells consisting of 2 O at 1.89 Å and 3 N at 2.07 Å. While the two shell fit is clearly a better mimic for the features of the EXAFS, the improvement is not statistically significant. The mean-square deviation between the data and the fit decreases by ca. 33% on going from one shell to two shells. The reduction is not significant, given that the two shell fit contains double the number of variable parameters. The failure of the two shell model to give a significant improvement is typical of the results found for low symmetry sites (Riggs-Gelasco, Stemmler, and Penner-Hahn, submitted to *Coord. Chem. Rev.*) This reflects the fact that, within the small-disorder approximation (i.e., eq 3), it is not possible to model the data using two resolvable shells. The true atomic distribution is best described by three or more shells of scatterers [see Lah et al. (1995)]. However, there are too few degrees of freedom in the present data to justify multiple shell analyses. It is noteworthy that the average bond length for the two shell fit is the same as that found in the one shell fit. Thus regardless of the model chosen, the *average* first shell bond length is well defined. The curve fitting results for the overall averages for the ferric enzyme at pH 7, at pH 9.4, at pH 10.5, and for the azide complex at pH 7 are given in Table 2.

Ferrous complexes typically have bond lengths 0.10−0.15 Å longer than the corresponding ferric complexes. It is thus possible that the photoreduction observed for the ferric pH 7 and ferric + azide samples could artifactually increase the average iron−ligand bond length. In order to determine the

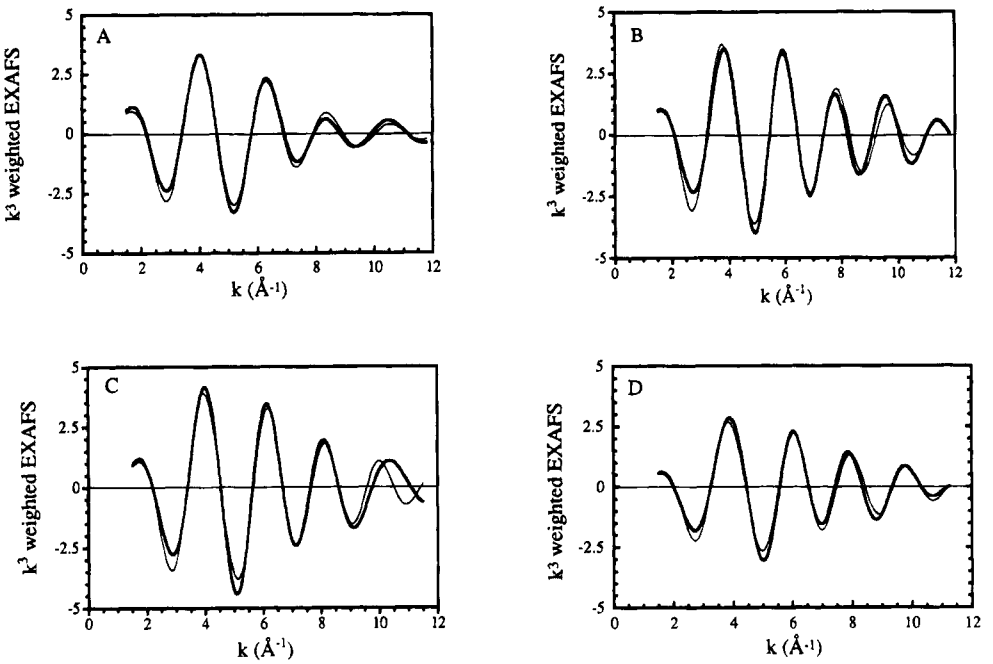

FIGURE 6: Fits to Fourier filtered EXAFS data. The fits are for filtered first shell data and do not include contributions from outer shells. The bold lines represent the data and the light lines represent the fits. (A) Ferric, pH 7 (two shell fit shown). (B) Ferric + azide. (C) Ferric, pH 9.4. (D) Ferric, pH 10.5.

effect of photoreduction on the apparent bond length, each data set was divided into thirds chronologically, and each third was fit separately. Refined bond lengths were found to increase monotonically by 0.006−0.012 Å from the first to last third of individual data sets. The one-third averages gave nearly identical values of σ^2, which increased marginally from the first third to the overall average. The bond lengths reported in Table 2 were obtained by extrapolating the fitting results to zero exposure. The correction relative to the bond length obtained neglecting photoreduction is 0.018 and 0.007 Å, respectively, for the ferric pH 7 and ferric + azide. This small correction is consistent with that expected for a data set that represents, on average, 10% reduced protein. The high pH samples showed no evidence for photoreduction and were not corrected.

DISCUSSION

The X-ray absorption near edge structure (XANES) region for Fe(III) complexes has been shown to be sensitive to geometry (Roe et al., 1984). The 1s→3d pre-edge transition of first row transition metals is a dipole forbidden transition which gains intensity from the admixture of 4p character with the metal 3d orbitals. The extent of mixing, and consequently the intensity of the 1s→3d transition, depends on the extent of the distortion from a centrosymmetric metal site. In general, intensity increases from six-coordinate pseudooctahedral ($<10 \times 10^{-2}$ eV) through five-coordinate ($12-19 \times 10^{-2}$ eV) to four-coordinate pseudotetrahedral ($>23 \times 10^{-2}$ eV), and the effect has been used to deduce coordination number (Roe et al., 1984). It is important to note, however, that the 1s→3d intensity is really a reflection of geometry rather than coordination number. Thus, the 1s→3d intensity in $CuCl_4^{2-}$ changes 7-fold on going from a square-planar site to a distorted tetrahedral site (Shadle et al., 1993).

The integrated area of the isolated 1s→3d transition (Table 2) for FeSOD at pH 7 is consistent with a pentacoordinate iron. There are no published examples of a four-coordinate Fe(III) having a 1s→3d transition area less than 23×10^{-2} eV. Although distortion toward a square planar structure could, in principle, give the observed area for a four coordinate Fe, there is no evidence for such a distortion in the *E. coli* (Stallings et al., 1983) crystal structure. The apparent EXAFS coordination number is also most consistent with a five-coordinate Fe, although it is difficult to determine coordination number precisely by EXAFS. Finally, the average bond length of 1.98 Å provides further evidence that Fe(III)SOD has a five-coordinate iron site.[3] A substantially shorter Fe−ligand bond distance would be expected for a four-coordinate Fe(III). All of these data support the proposal that a fifth ligand, presumably a solvent molecule, is bound to the iron in solutions of *E. coli* Fe(III)SOD at pH 7.

The apparent EXAFS bond lengths (Table 2) are a slight underestimate of the true average Fe−ligand distances. Since there are insufficient data to resolve two shells of scatterers (see above), the first shell data were fit with Fe−N parameters. When Fe−N parameters are used to fit Fe−O scattering, the bond length is underestimated by 0.02−0.03 Å due to the differences in EXAFS phase shifts for oxygen and nitrogen. Since the different FeSOD derivatives are known to have three or four nitrogen and two or three oxygen ligands, the apparent bond lengths are all 0.01−0.02 Å shorter than the true average bond lengths. With or without this correction, the average bond lengths reported here are in excellent agreement with those obtained by Lah et al. (1995) thus confirming that this crystal structure is a good description of the metal site structure of the *E. coli* protein in solution. However, the EXAFS bond length at pH 7 differs substantially from the average of 2.4 Å (Stoddard et al., 1990b) found crystallographically for the *P. ovalis* protein at pH 4.8, the pH of crystallization.

From the crystal structure, it is clear that there must be at least two, and probably more, shells of scatterers in the first

coordination sphere about the iron. Within the present resolution limits it is not possible to resolve the different shells. However, evidence for the presence of multiple shells is found in the magnitude of the Debye−Waller factor, σ^2. The observed σ^2 is the sum of σ^2_{vib} and σ^2_{static}, the thermal and structural contributions to the disorder. For Fe−(N/O) bonds at 10−20 K, the σ^2_{vib} contribution should be negligible. There is a substantial uncertainty in EXAFS determination of σ^2 due to the correlation between σ^2 and the coordination number and due to the breakdown of the small disorder approximation in eq 3. Nevertheless, if the σ^2 values in Table 2 are taken as σ^2_{static}, the apparent spread in bond lengths for a two shell distribution is ~0.15−0.20 Å. This is completely consistent with the crystallographic distances (σ^2_{static} for the ferric pH 7 and the ferric pH 7 + azide, calculated from the crystallographic distances, are 9.6×10^{-3} and 6.1×10^{-3} Å^2, respectively).

On addition of azide, the 1s→3d area decreases to a value typical of six-coordinate Fe(III) complexes. The observed decrease in intensity is larger than the variability in the measurement, indicating that the difference is significant. The apparent EXAFS coordination number increases to six, and the average Fe−ligand bond length increases by 0.08 Å. All of these changes point to an increase in the coordination number of the iron when azide binds. The 1s→3d area is in excellent agreement with that expected for a six-coordinate iron site and is significantly smaller than any reported for a five-coordinate Fe(III). These data thus demonstrate that azide binds directly to the Fe(III) and that this binding occurs without loss of either protein or solvent ligands. Once again, the EXAFS data are in excellent agreement with the crystal structure of the *E. coli* enzyme.

The XAS data for the high pH samples suggest that the pH-dependent structural transition which occurs in ferric SOD (Fee et al., 1981; Stallings et al., 1991) corresponds to expansion of the iron coordination sphere. The increase in average bond length on going from pH 7 to 10.5 is consistent with that expected for an increase in coordination number from five to six. Indeed, the first shell bond length at pH 10.5 is identical to that obtained for the azide complex. The average bond length for the pH 9.4 sample is consistent with a mixture of bound (six-coordinate) and unbound (five-coordinate) iron sites. If the apparent bond length for the pH 9.4 sample, 2.03 Å, is taken to be the weighted average of a low pH form having five ligands at an average distance of 1.98 Å and a high pH form with six ligands at an average distance of 2.06 Å, the apparent composition is ~40% low pH form and 60% high pH form. This ratio, in turn, implies a pK_a value of 9.3, which is in good agreement with the pK_a value obtained from fitting the XANES data (9.8) and with the values obtained from other methods. Previous UV−vis, EPR, and activity measurements for Fe(III)SOD had suggested a pH-dependent structural change with a pK_a of 9.0 ± 0.3. However, more recent Mössbauer results suggest the iron is only 70% converted to the high pH form at pH 10 (Niederhoffer et al., 1987). Seventy percent conversion at pH 10 indicates a pK_a of approximately 9.6. The excellent agreement between these pK_a values suggests that these observations all monitor the same transition.

The 1s→3d line width has been shown to increase with increasing coordination number for a number of ferric complexes (Roe et al., 1984). The breadth of this transition at elevated pH is likely to lead to greater uncertainty in background subtraction, and consequently, to greater uncertainty in integration of the peak areas. This is the most likely explanation of a 1s→3d area of 15 for a site that we have assigned as six coordinate. Alternatively, the larger areas obtained for the pH 9.9 and 10.5 samples could be due to greater distortion of the iron site. For example, a more distorted site, caused by binding of a pair of *cis*-hydroxides, might compensate for the increase in coordination number to give the observed 1s→3d intensities at elevated pH.

The XAS data suggest that the spectroscopic changes observed previously above pH 9 are likely to result from binding of hydroxide as a sixth ligand. Deprotonation of a distant group would be expected to have little effect on the EXAFS of the iron site, while deprotonation of bound water should, at most, serve to slightly decrease the average bond length. The observed increase in average bond length is more likely to result from addition of a sixth ligand, presumably hydroxide.[4] These data provide the first direct structural evidence for a six-coordinate iron site at high pH. Competition between hydroxide ion and other anions for an open coordination site would explain the pH dependence of both K_m and azide binding above pH 8 (Bull & Fee, 1985).

The 350 nm absorption band, which has been assigned as a ligand to metal charge transfer transition (Slykhouse & Fee, 1976), has negligible intensity above pH 9. Fluoride ion has been shown to cause a similar bleaching of this band while binding of azide, a relatively soft ligand, leads to a red-shift of λ_{max} for this transition (Slykhouse & Fee, 1976; Fee et al., 1981; Bull & Fee, 1985). Our interpretation predicts that the charge transfer of the high pH complex may be blue-shifted by the addition of a relatively hard hydroxide ligand.

Neither EXAFS nor crystallography can be used to determine directly whether the solvent molecule bound to ferric SOD is protonated (i.e., H_2O) or deprotonated (i.e., OH^-) at pH 7. Similarly, kinetic studies show that a single proton is linked to the high pH conversion but cannot distinguish between deprotonation of a previously bound water and binding of exogenous hydroxide. However, with our finding that a sixth ligand is bound at high pH, it appears that the solvent molecule in the ferric pH 7 enzyme must already be deprotonated. In order to be bound as water and to remain protonated up to pH 10, the solvent molecule would have to have a pK_a > 11. In contrast, the pK_a of water typically decreases from 14 to ~2 on binding to Fe(III) (Huheey, 1983).

It is known that reduction of FeSOD is coupled to the uptake of one proton (Bull & Fee, 1985). If the solvent molecule in the ferric enzyme is in fact deprotonated at pH 7, it becomes a likely candidate for the group that is protonated on reduction. This would be consistent with the expected increase in the pK_a for water bound to Fe(II), ~10, relative to water bound to Fe(III), ~2, as a consequence of the decreased Lewis acidity of Fe(II).

Conclusions. Ferric superoxide dismutase from *E. coli* is five-coordinate in its resting state at pH 7. This provides independent confirmation of the crystallographic model of Lah et al. (1995) and is incosistent with the Fe-site geometry

[4] Addition of a protein derived ligand would also be consistent with the data. However, the nearest potential ligand is a tyrosine whose closest approach is ca. 4 Å with significant rearrangement of the protein backbone (M. Ludwig, unpublished data).

proposed on the basis of the crystal structure of the *Ps. ovalis* enzyme (Stoddard et al., 1990a). Addition of azide or an increase in pH both convert the iron to a six-coordinate structure, demonstrating that azide binding and high pH conversion are not accompanied by loss of the bound solvent. This is consistent with a model in which the bound water acts as a proton acceptor during the reductive half-reaction.

ACKNOWLEDGMENT

We thank Ms. Anita Metzger for her assistance in sample preparation. We also thank Dr. Stephen P. Cramer for use of the 13-element detector array and Dr. James O. Alben for use of the Oxford cryostat on beamline X19A.

REFERENCES

Autor, A. P. (1982) *J. Biol. Chem. 257*, 2713.

Borgstahl, G. E. O., Parge, H. E., Hickey, M. J., Beyer, W. F. B., Jr., Hallewell, R. A., & Tainer, J. A. (1992) *Cell 71*, 107−118.

Bull, C., & Fee, J. A. (1985) *J. Am. Chem. Soc. 107*, 3295−3304.

Carlioz, A., Ludwig, M. L., Stallings, W. C., Fee, J. A., Steinman, H. M., & Touati, D. (1988) *J. Biol. Chem. 263*, 1555−1562.

Dooley, D. M., Jones, T. F., Karas, J. L., McGuirl, M. A., Brown, R. D., III, & Koenig, S. H. (1987) *J. Am. Chem. Soc. 109*, 721−725.

Fee, J. A., McClune, G. J., Lees, A. C., Zidovetski, R., & Pecht, I. (1981) *Isr. J. Chem. 21*, 54−58.

Huheey, J. E. (1983) *Inorganic Chemistry*, Harper and Row, New York.

Lah, M. S., Dixon, M. M., Pattridge, K. A., Stallings, W. C., Fee, J. A., & Ludwig, M. L. (1995) *Biochemistry 34*, 1646−1660.

Ludwig, M. L., Metzger, A. L., Pattridge, K. A., & Stallings, W. C. (1991) *J. Mol. Biol. 219*, 335−358.

McCord, J. M., & Fridovich, I. (1969) *J. Biol. Chem. 244*, 6049−6055.

McMaster, W. H., Kerr del Grande, N., Mallett, J. H., & Hubbell, J. H. (1969) *Combination of X-Ray Cross Sections*, Lawrence Radiation Laboratory, Livermore, CA.

Niederhoffer, E. C., Fee, J. A., Papaefthymiou, V., & Munck, E. (1987) *Isotope and Nuclear Chemistry Division Annual Report, Los Alamos National Lab*, 79−85.

Rehr, J., & Zabinsky, A. (1991) *J. Am. Chem. Soc. 113*, 5135−5140.

Ringe, D., Petsko, G. A., Yamakura, F., Suzuki, K., & Ohmori, D. (1983) *Proc. Natl. Acad. Sci. U.S.A. 80*, 3879−3863.

Roberts, V. A., Fisher, C. L., Redford, S. M., McRee, D. E., Parge, H. E., Getzoff, E. D., & Tainer, J. A. (1991) *Free Rad. Res. Commun. 12−13*, 269−278.

Roe, A. L., Schneider, D. J., Mayer, R. J., Pyrz, J. W., Widom, J., & Que, L., Jr. (1984) *J. Am. Chem. Soc. 106*, 1676.

Sato, S., & Nakasawa, K. (1978) *J. Biochem. (Tokyo) 83*, 1165.

Shadle, S. E., Penner-Hahn, J. E., Schugar, H. J., Hedman, B., Hodgson, K. O., & Solomon, E. I. (1993) *J. Am. Chem. Soc. 115*, 767−76.

Shannon, R. D. (1976) *Acta Crystallogr. A32*, 751−767.

Slykhouse, T. O., & Fee, J. A. (1976) *J. Biol. Chem. 251*, 5472−5477.

Stallings, W. C., Powers, T. B., Pattridge, K. A., Fee, J. A., & Ludwig, M. L. (1983) *Proc. Natl. Acad. Sci. U.S.A. 80*, 3884−3888.

Stallings, W. C., Pattridge, K. A., Strong, R. K., & Ludwig, M. L. (1985) *J. Biol. Chem. 260*, 16424−16432.

Stallings, W. C., Metzger, A. L., Pattridge, K. A., Fee, J. A., & Ludwig, M. L. (1991) *Free Rad. Res. Commun. 12−13*, 259−268.

Stallings, W. C., Bull, C., Fee, J. A., Lah, M. S., & Ludwig, M. L. (1992) *Molecular Biology of Free Radical Scavenging Systems*, Cold Spring Harbor Lab Press, Cold Spring Harbor, NY.

Stoddard, B. L., Howell, P. L., Ringe, D., & Petsko, G. A. (1990a) *Biochemistry 29*, 8885−8893.

Stoddard, B. L., Ringe, D., & Petsko, G. A. (1990b) *Protein Eng. 4*, 113−119.

Thorp, H. H. (1992) *Inorg. Chem. 31*, 1585−8.

Villafranca, J. J. (1976) *FEBS Lett. 62*, 230−232.

Waldo, G. S. (1991) Ph.D. Thesis, The University of Michigan, Ann Arbor, MI.

BI9415154